

Time-efficient Joint Chance-constrained Optimal Power Flow with a Learning-based Robust Approximation

Ge Chen, *Graduate Student Member, IEEE*, Hongcai Zhang, *Member, IEEE*, Hongxun Hui, *Member, IEEE*, and Yonghua Song, *Fellow, IEEE*

Abstract—With the increasing penetration of renewable generation integrated into power networks, how to manage uncertainties in optimal power flow (OPF) has become a major concern for network operators. This paper proposes a joint chance-constrained OPF model to tackle uncertainties. This model jointly guarantees the satisfaction probability of all critical OPF constraints so that it can effectively ensure the feasibility of OPF solutions. Considering that the existing works for handling joint chance constraints (JCCs) are either overly conservative or computationally intractable, we propose a time-efficient learning-based robust approximation method for JCCs. It first adopts the sample average approximation (SAA) to convert JCCs into sample-wise constraints with binary variables. Then, the One-Class Support Vector Clustering is introduced to pre-solve the binary variables in SAA. To further improve the computational performance, we design a robust approximation to replace the large number of sample-wise constraints with only a few robust constraints. As a result, the original complex joint chance-constrained OPF model is formulated into a simple linear form. Moreover, since the proposed model is data-driven, it is applicable to arbitrarily distributed uncertainties. Numerical experiments are conducted to validate the superiority of the proposed method on optimality, feasibility, and computational efficiency.

Index Terms—Optimal power flow, joint chance constraints, machine learning, uncertainty set, distribution networks.

I. INTRODUCTION

OPTIMAL power flow (OPF) plays a key role in distribution network operations [1]. Every day, network operators need to solve OPF many times to optimize the power dispatch for controllable devices in systems. However, since stochastic distributed renewable generation (DRG) has been integrated into distribution networks, considerable uncertainties have been introduced [2]. Thus, managing uncertainties becomes a crucial task in OPF.

Chance-constrained programming (CCP) is a promising approach to handle uncertainties in OPF. Unlike robust optimization requiring that every constraint should be satisfied for all possible realizations of uncertainties, low-probability constraint violations are allowed in CCP [3]. Therefore, CCP can better balance the risk and economy. Many published works have introduced CCP to handle uncertainties in OPF. For example, reference [4] developed a chance-constrained optimal power flow (CC-OPF) model to describe Gaussian uncertainties from wind generation. Reference [5] adopted the CC-OPF to promote the integration of DRG in distribution networks. Reference [6] combined the CC-OPF with the Gaussian mixture model to handle constraints with non-Gaussian uncertainties. In [7], a CC-OPF model was presented to coordinate natural gas systems with power systems. However, most

of them, including [4]–[7], used individual chance constraints (ICCs) to describe the probabilistic satisfaction requirement of the power flow constraints under uncertainties, which can not effectively ensure the joint satisfaction of critical constraints of the entire system with a pre-determined probability [8].

For a power network operator, all security constraints should be jointly considered to guarantee the whole system's safe operation. Therefore, joint chance constraint (JCCs), which jointly describe the violation probability of all security constraints, are preferable. However, JCCs are usually intractable [9]. The published methods to tackle JCCs in OPF can be generally divided into the following three categories.

1) *Bonferroni approximation*: The Bonferroni approximation is a popular decomposition method [8] that can decompose an intractable JCC into multiple tractable ICCs. References [10], [11] employed this method to approximate JCCs with multiple ICCs for AC OPF problems. Reference [12] utilized this method to minimize the investment of the natural gas network considering demand uncertainties. References [13], [14] provided a tighter upper bounds to improve its OPF solutions' optimality. Nevertheless, since it requires that the summation of the risk parameters in all ICCs should be smaller than the original risk parameter in the JCC, its solutions are usually overly conservative, especially when the number of jointly considered constraints is large [15].

2) *Scenario approach*: The Scenario approach approximates JCCs by requiring the corresponding constraints to be robust for a finite number of scenarios. Here a scenario refers to one randomly selected sample. If the considered scenarios size is large enough, the feasibility of the original JCC can be guaranteed [3]. Reference [16] utilized the scenario approach to reformulate JCCs for AC OPF. Reference [17] applied the scenario approach to convexify the JCCs in a unit commitment problem. However, this approach usually introduces numerous scenarios so that it can be computationally expensive. To address this challenge, references [18], [19] designed uncertainty sets to cover all scenarios, and converted scenario-wise constraints into a single robust constraint. Nevertheless, their solutions may be overly conservative once some extreme samples are chosen.

3) *Sample average approximation*: Sample Average Approximation (SAA) also deals with JCCs based on samples [20]. SAA first utilizes a large enough empirical sample set to approximate the underlying true distribution of uncertainties. Then, it introduces auxiliary binary variables to identify safe samples (that satisfy all constraints) and unsafe samples (that violate some constraints). By restricting the unsafe sample

number to be smaller than a given value, JCCs can be approximated by sample-wise deterministic constraints with binary variables. The main difference between the aforementioned scenario approach and SAA is that the former does not accept any constraint violation for any scenario, while the latter allows some unsafe samples. Thus, SAA has the potential to achieve better optimality [3]. SAA has been utilized to handle JCCs in power grid planning [21] and unit commitment [22]. Nevertheless, because SAA usually introduces a large number of binary variables, it is also computationally expensive.

To overcome the aforementioned challenges, this paper proposes a time-efficient joint chance-constrained OPF model, which can jointly consider satisfaction of all OPF constraints. The key contribution of this paper is a novel learning-based robust approximation method for the joint chance-constrained OPF model. This approximation includes the following three major steps: First, it adopts SAA to convert one JCC into sample-wise constraints with binary variables. Second, the One-Class Support Vector Clustering (OC-SVC) is introduced to identify safe and unsafe samples so that the aforementioned binary variables can be determined in advance. Third, a minimum volume box uncertainty set is constructed to cover all the safe samples. After that, the large scale sample-wise constraints can be replaced by a small number of robust constraints. As a result, the proposed joint chance constrained OPF is approximated by a simple robust linear programming. Moreover, since the proposed model is a data-driven approach, it can be applied to JCCs with arbitrary distributed uncertainties. Numerical experiments prove the superiority of the proposed method on optimality, feasibility, and computational efficiency.

The remaining parts are organized as follows. Section II formulates the joint chance constrained model. Section III proposes the robust approximation. Section IV illustrates simulation results and Section V concludes this paper.

II. PROBLEM FORMULATION

We consider a distribution network operator solves an OPF problem with strategic power scheduling of renewable generators, e.g., wind turbines (WTs), and flexible resources, e.g., energy storage systems (ESSs). The operator requires that all OPF constraints shall be jointly satisfied with a predetermined confidence level to ensure feasibility of the solutions with arbitrary distributions of uncertainties.

A. Basic optimal power flow model

1) *Operation objective*: The objective of OPF is to minimize the expected total energy cost of the distribution network:

$$\min \sum_{t \in \mathcal{T}} EC_t, \quad (1)$$

where EC_t represents the system energy cost at time $t \in \mathcal{T}$, which is defined as:

$$EC_t = (\eta^{\text{buy}} G_t^{\text{buy}} - \eta^{\text{sell}} G_t^{\text{sell}}) \Delta t, \quad \forall t \in \mathcal{T}, \quad (2)$$

$$G_t^{\text{buy}} - G_t^{\text{sell}} = G_t^g, \quad G_t^{\text{buy}} \geq 0, \quad G_t^{\text{sell}} \geq 0, \quad \forall t \in \mathcal{T}, \quad (3)$$

where η^{buy} and η^{sell} are the per-unit prices of electricity purchasing and selling, in \$/kWh, respectively; G_t^{buy} and G_t^{sell} are the electricity purchasing and selling; variable G_t^g is the net load at the substation and Δt is the length of a time slot.

2) *Power flow constraints*: We employ the widely used linearized DistFlow model [23] to describe the power flows in distribution networks, as follows:

$$\begin{cases} P_{ij,t} = \sum_{k \in \mathcal{C}_j} P_{jk,t} - p_{j,t}, \\ Q_{ij,t} = \sum_{k \in \mathcal{C}_j} Q_{jk,t} - q_{j,t}, \quad \forall (i,j) \in \mathcal{B}, \forall t \in \mathcal{T}, \\ U_{j,t} = U_{i,t} - 2(r_{ij} P_{ij,t} + x_{ij} Q_{ij,t}), \end{cases} \quad (4)$$

where $P_{ij,t}$ and $Q_{ij,t}$ denote the active and reactive power flows on branch $(i,j) \in \mathcal{B}$, respectively; symbols i and j are the bus indexes, $(i,j) \in \mathcal{V}$; $p_{j,t}$ and $q_{j,t}$ are the active and reactive power injections at bus j , respectively; U_i is the square of the voltage at bus i ; r_{ij} and x_{ij} are the resistance and reactance of branch (i,j) , respectively; set \mathcal{C}_j contains the child bus indexes of bus j , $\mathcal{C}_j \subseteq \mathcal{V}$. The net power at substation G_t^g is equal to the summation of the active power flows from the slack bus (indexed by $i = 0$) to all its child buses, as follows:

$$G_t^g = \sum_{j \in \mathcal{C}_0} P_{0j,t}, \quad \forall t \in \mathcal{T}. \quad (5)$$

Eq. (4) can be further expressed in a matrix form, as follows:

$$\mathbf{p}_t = \mathbf{A}^T \mathbf{P}_t, \quad \mathbf{q}_t = \mathbf{A}^T \mathbf{Q}_t, \quad \forall t \in \mathcal{T}, \quad (6)$$

$$\mathbf{U}_t = U_{0,t} \mathbf{1} - 2(\mathbf{R} \mathbf{p}_t + \mathbf{X} \mathbf{q}_t), \quad \forall t \in \mathcal{T}. \quad (7)$$

Symbols $\mathbf{p}_t \in \mathbb{R}^{|\mathcal{V}|}$, $\mathbf{q}_t \in \mathbb{R}^{|\mathcal{V}|}$, $\mathbf{U}_t \in \mathbb{R}^{|\mathcal{V}|}$ are the vector forms of $p_{i,t}$, $q_{i,t}$ and $U_{i,t}$, $\forall i \in \mathcal{V}$; \mathbf{A} is the reduced branch-bus incidence matrix, which is obtained by removing the first column from the original branch-bus incidence matrix [24]; $\mathbf{P}_t \in \mathbb{R}^{|\mathcal{B}|}$ and $\mathbf{Q}_t \in \mathbb{R}^{|\mathcal{B}|}$ are the vector forms of $P_{ij,t}$ and $Q_{ij,t}$, $\forall (i,j) \in \mathcal{B}$; R_{ij} and X_{ij} are the entries of matrices \mathbf{R} and \mathbf{X} , respectively. They are defined as the summation of resistances and reactances of all common branches between the two paths from the root bus 0 to buses i and j , e.g., if the paths from bus 0 to buses 2 and 3 are $\{(0,1), (1,2)\}$ and $\{(0,1), (1,2), (2,3)\}$, respectively; then $R_{23} = r_{01} + r_{12}$.

All bus voltages and branch power flows should lie in a proper range to ensure the system security, as follows:

$$\mathbf{U}_{\min} \leq \mathbf{U}_t \leq \mathbf{U}_{\max}, \quad \forall t \in \mathcal{T}, \quad (8)$$

$$P_{ij,t}^2 + Q_{ij,t}^2 \leq (S_{ij}^{\max})^2, \quad \forall (i,j) \in \mathcal{B}, \forall t \in \mathcal{T}, \quad (9)$$

where S_{ij}^{\max} is the maximum allowable apparent power flow on branch (i,j) .

3) *Power balance constraints*: The power injection \mathbf{p}_t and \mathbf{q}_t on each bus can be expressed as:

$$\mathbf{p}_t = (\mathbf{p}_t^{\text{dis}} - \mathbf{p}_t^{\text{cha}}) - \mathbf{p}_t^{\text{PD}} + \mathbf{p}_t^{\text{WT}} * \boldsymbol{\lambda}_t, \quad \forall t \in \mathcal{T}, \quad (10)$$

$$\mathbf{q}_t = -\mathbf{q}_t^{\text{PD}} + \boldsymbol{\psi}_t * \mathbf{p}_t^{\text{WT}} * \boldsymbol{\lambda}_t, \quad \forall t \in \mathcal{T}, \quad (11)$$

$$\mathbf{0} \leq \boldsymbol{\lambda}_t \leq \mathbf{1}, \quad \forall t \in \mathcal{T}, \quad (12)$$

where $\mathbf{p}_t^{\text{cha}}$ and $\mathbf{p}_t^{\text{dis}}$ are the charging and discharging powers of ESSs; \mathbf{p}_t^{WT} and $\boldsymbol{\lambda}_t$ are the available wind power and corresponding actual utilization rate; operator $*$ represents the

elementwise multiplication; \mathbf{p}_t^{PD} and \mathbf{q}_t^{PD} represent the active and reactive power demands on each bus; ψ_t is the ratio of WTs' active power outputs to their reactive power outputs.

The charging and discharging powers affects the energy stored in ESSs, as follows:

$$\mathbf{E}_t = \mathbf{E}_{t-1} + (\eta^{\text{cha}} \mathbf{p}_{t-1}^{\text{cha}} - \mathbf{p}_{t-1}^{\text{dis}} / \eta^{\text{dis}}) \Delta t, \quad \forall t \in \mathcal{T}, \quad (13)$$

where \mathbf{E}_t represents the energy stored in ESSs at time t ; η^{cha} and η^{dis} are efficiency coefficients for power charging and discharging. Due to the device limitation, both the energy stored in ESSs and charging/discharging power are bounded:

$$\mathbf{E}^{\min} \leq \mathbf{E}_t \leq \mathbf{E}^{\max}, \quad \mathbf{0} \leq \mathbf{p}_t^{\text{cha}}, \mathbf{p}_t^{\text{dis}} \leq \mathbf{p}^{\max}, \quad \forall t \in \mathcal{T}. \quad (14)$$

Finally, the deterministic OPF problem can be formulated as:

$$\begin{aligned} & \min_{\mathbf{p}_t^{\text{dis}}, \mathbf{p}_t^{\text{cha}}, \boldsymbol{\lambda}_t, \forall t \in \mathcal{T}} \quad \text{Eq. (1)}, \\ & \text{s.t.} \quad \text{Eqs. (2)-(3), and (5)-(14)}. \end{aligned} \quad (\text{P1})$$

B. Chance-constrained OPF with uncertainties

The real wind power is uncertain, and can be expressed as¹:

$$\mathbf{p}_t^{\text{WT}} = \bar{\mathbf{p}}_t^{\text{WT}} * (1 + \boldsymbol{\omega}_t), \quad \forall t \in \mathcal{T}, \quad (15)$$

where $\bar{\mathbf{p}}_t^{\text{WT}}$ and $\boldsymbol{\omega}_t$ are the available wind power forecast and uncertain level, respectively. According to Eqs. (10)-(11), the uncertainty $\boldsymbol{\omega}$ from the wind power affects the power injections on each bus. Based on the power flow model (6)-(7), this uncertainty further propagates to the square of the bus voltage \mathbf{U}_t , branch power flows \mathbf{P}_t and \mathbf{Q}_t . Thus, the impacts of this uncertainty must be considered in the OPF model; otherwise, the obtained OPF solutions may be infeasible for (8)-(9).

Traditionally, robust optimization is used to handle the uncertainty. However, the solution of robust optimization is usually overly conservative. To better balance optimality and robustness, CCP is employed to describe the inequality constraints under uncertainties, including Eqs. (8) and (9):

$$\mathbb{P}(\text{Eqs. (8)-(9)}) \geq 1 - \epsilon, \quad \forall t \in \mathcal{T}, \quad (16)$$

where ϵ is the risk parameter.

Remark 1. We use JCCs instead of multiple ICCs to restrict the violation probability of the security constraints (8) and (9) under uncertainties. This joint manner is preferable for network operators because it can ensure the solution's feasibility for the entire system with a pre-determined confidence level.

JCC (16) contains quadratic constraints, i.e., Eq. (9), in its probability operator, which are intractable. To address this, we introduce two auxiliary variables $P_{ij,t}^{\text{aux}}$ and $Q_{ij,t}^{\text{aux}}$ to extract these quadratic constraints from the probability operator:

$$(P_{ij,t}^{\text{aux}})^2 + (Q_{ij,t}^{\text{aux}})^2 \leq (S_{ij}^{\max})^2, \quad \forall (i, j) \in \mathcal{B}, \quad (17)$$

$$\mathbb{P} \left(\begin{array}{l} \mathbf{U}_{\min} \leq \mathbf{U}_t \leq \mathbf{U}_{\max}, \\ |P_{ij,t}| \leq P_{ij,t}^{\text{aux}}, \forall (i, j) \in \mathcal{B}, \\ |Q_{ij,t}| \leq Q_{ij,t}^{\text{aux}}, \forall (i, j) \in \mathcal{B}, \end{array} \right) \geq 1 - \epsilon, \forall t \in \mathcal{T}. \quad (18)$$

¹Here we only consider the uncertainties from wind power, but the proposed model can be also easily extended to involve other uncertain sources (e.g. demands) by adding corresponding random variables in the system model.

Obvious, Eqs. (17) and (18) are an inner approximation of the original JCC (16). Finally, we can formulate the chance-constrained OPF with JCCs as:

$$\begin{aligned} & \min_{\mathbf{x}_t, \forall t \in \mathcal{T}} \quad \text{Eq. (1)}, \\ & \text{s.t.} \quad \text{Eqs. (2)-(3), (5)-(7), (10)-(14), and (17)-(18)}, \end{aligned} \quad (\text{P2})$$

where $\mathbf{x}_t = \{\mathbf{p}_t^{\text{dis}}, \mathbf{p}_t^{\text{cha}}, \boldsymbol{\lambda}_t, \mathbf{P}_t^{\text{aux}}, \mathbf{Q}_t^{\text{aux}}\}$ are decision variables.

III. SOLUTION METHODOLOGY

To overcome the challenges mentioned in Section I, this section designs a novel learning-based robust approximation method for the intractable JCC (18). Specifically, we first apply the SAA to reformulate JCC (18) into a mixed-integer form. Then, a learning-based robust approximation is proposed to convert the previous mixed-integer programming into a linear one, which guarantees computational tractability.

A. SAA-based Reformulation of JCC

SAA uses the discrete historical samples of uncertainties to approximate the underlying true distribution. Next, we use JCC (18) as an example to demonstrate how SAA works. We omit the subscript t for convenience.

1) *Basic form of SAA:* Observing that all constraints inside the probability operator in Eq. (18) are linear, they can be written into a generic form, as follows:

$$\mathbf{a}_m(\mathbf{x})^\top \boldsymbol{\omega} \leq b_m(\mathbf{x}), \quad \forall m \in \mathcal{M}, \quad (19)$$

where $\mathbf{a}_m(\mathbf{x})$ is the uncertainty coefficient in the m -th constraint inside the probability operator; $b_m(\mathbf{x})$ is the term that is independent of uncertainty $\boldsymbol{\omega}$; \mathcal{M} is the index set of constraints, where its length $|\mathcal{M}| = 2|\mathcal{V}| + 4|\mathcal{B}|$. By defining function $h(\mathbf{x}, \boldsymbol{\omega})$ as:

$$h(\mathbf{x}, \boldsymbol{\omega}) = \max\{\mathbf{a}_m(\mathbf{x})^\top \boldsymbol{\omega} - b_m(\mathbf{x}), \forall m \in \mathcal{M}\}, \quad (20)$$

the intractable JCC (18) can be written as a simple form:

$$\mathbb{P}(h(\mathbf{x}, \boldsymbol{\omega}) \leq 0) \geq 1 - \epsilon \Leftrightarrow \mathbb{P}(h(\mathbf{x}, \boldsymbol{\omega}) \geq 0) \leq \epsilon. \quad (21)$$

Suppose we have $|\mathcal{N}|$ historical samples of $\boldsymbol{\omega}$ (indexed by $n \in \mathcal{N}$), then SAA approximates Eq. (21) by:

$$\frac{1}{|\mathcal{N}|} \sum_{n \in \mathcal{N}} \mathbb{1}(h(\mathbf{x}, \boldsymbol{\omega}^{(n)}) \geq 0) \leq \epsilon^{\text{SAA}}, \quad (22)$$

where $\mathbb{1}(\cdot)$ is an indicator function: If the inside statement is true, $\mathbb{1}(\cdot) = 1$; otherwise, $\mathbb{1}(\cdot) = 0$. Symbol ϵ^{SAA} denotes the risk parameter, which is different from ϵ in Eq. (21). Note that Eq. (22) is still intractable because off-the-shelf solvers can not directly handle the indicator function.

2) *Feasibility guarantee:* The empirical distribution formed by the historical samples may differ from the underlying true one. If we set $\epsilon^{\text{SAA}} = \epsilon$, then a feasible solution to the SAA form (22) may be infeasible for the original JCC (21). Thankfully, the following **Lemma** provide a simple way to determine ϵ^{SAA} with guaranteed feasibility.

Lemma 1. The solution to the SAA form (22) with $\epsilon^{\text{SAA}} = J/|\mathcal{N}|$ is feasible to the original JCC (21) with probability at

least $1 - \beta$, where J is the largest integer that can satisfy the following inequality:

$$\binom{J+D_x-1}{J} \sum_{j=0}^{J+D_x-1} \binom{|M|}{j} \epsilon^j (1-\epsilon)^{|M|-j} \leq \beta, \quad (23)$$

where D_x is the dimension of \mathbf{x} [25].

Then, by choosing a small β , the SAA form (22) can guarantee the feasibility for the original JCC (21).

3) *Conventional reformulation of SAA*: Since off-the-shelf solvers can not directly handle the indicator function, we need to reformulate Eq. (22) into a solvable form. A conventional reformulation is based on the Big-M method, which convert Eq. (22) into a mixed-integer form:

$$\sum_{n \in \mathcal{N}} z_n \leq |\mathcal{N}| \cdot \epsilon^{\text{SAA}}, \quad (24)$$

$$h(\mathbf{x}, \boldsymbol{\omega}^{(n)}) \leq M z_n, \quad z_n \in \{0, 1\}, \quad \forall n \in \mathcal{N}, \quad (25)$$

where z_n is an auxiliary binary variable: If $z_n = 1$, then the n -th sample $\boldsymbol{\omega}^{(n)}$ is a unsafe sample, i.e., a sample violating $h(\mathbf{x}, \boldsymbol{\omega}^{(n)}) \leq 0$; otherwise, the n -th sample satisfies $h(\mathbf{x}, \boldsymbol{\omega}^{(n)}) \leq 0$. Parameter M is a big enough constant.

Remark 2. SAA provides an effective way to approximate JCCs. However, it needs to introduce $|\mathcal{N}|$ binary variables, leading to a huge computational burden.

B. Robust approximation of SAA based on OC-SVC

1) *Sample-wise robust approximation*: If we can distinguish the safe and unsafe samples, then the auxiliary binary variable z_n can be determined in advance. In this case, the mixed-integer constraints (24)-(25) degenerate into the following sample-wise constraints without any integer variable:

$$\begin{aligned} h(\mathbf{x}, \boldsymbol{\omega}^{(n)}) &\leq 0, \quad \forall n \in \mathcal{N}/\mathcal{N}^{\text{vio}}, \\ \Leftrightarrow \mathbf{a}_m(\mathbf{x})^\top \boldsymbol{\omega}^{(n)} &\leq b_m(\mathbf{x}), \quad \forall n \in \mathcal{N}/\mathcal{N}^{\text{vio}}, \quad \forall m \in \mathcal{M}, \end{aligned} \quad (26)$$

where \mathcal{N}^{vio} is the index set of all unsafe samples. Note Eq. (26) is equivalent to the following robust constraint:

$$\max_{\boldsymbol{\omega} \in \mathcal{U}^{\text{safe}}} \mathbf{a}_m(\mathbf{x})^\top \boldsymbol{\omega} \leq b_m(\mathbf{x}), \quad \forall m \in \mathcal{M}, \quad (27)$$

where the uncertainty set $\mathcal{U}^{\text{safe}}$ is composed of discrete samples and defined by $\{\boldsymbol{\omega}^{(n)}, \forall n \in \mathcal{N}/\mathcal{N}^{\text{vio}}\}$. According to Eq. (24), the length of \mathcal{N}^{vio} is constrained by:

$$|\mathcal{N}^{\text{vio}}| \leq |\mathcal{N}| \cdot \epsilon^{\text{SAA}}. \quad (28)$$

With different \mathcal{N}^{vio} , the corresponding optimality performances are also different. Thus, the key problem becomes how to identify safe and unsafe samples.

2) *Identifying safe/unsafe samples with OC-SVC*: We introduce OC-SVC [26], a famous anomaly detection algorithm, as a guideline to distinguish unsafe samples from safe samples. OC-SVC can find a sphere with minimum volume in a mapped space as the classification boundary to separate the unsafe samples and safe samples, as shown in Fig. 1. The corresponding training process is expressed by:

$$\min_{R, \mathbf{o}, \boldsymbol{\omega}} R^2 + \lambda \sum_{n \in \mathcal{N}} y_n, \quad (\text{P-SVC})$$

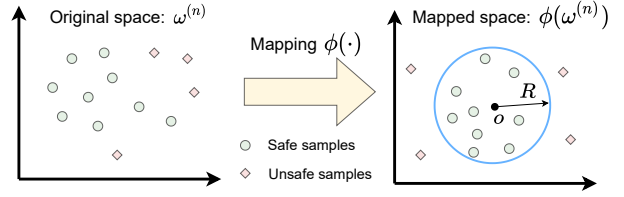


Fig. 1. Schematic diagram of OC-SVC. The green dots and pink diamonds represents safe and unsafe samples, respectively. The blue circle denotes the boundary of the minimum sphere in the mapped space, while variables R and \mathbf{o} are its radius and center.

TABLE I
CRITERION FOR DISTINGUISHING SAMPLES

Criterion	Positions	Categories
$\kappa_n = 0$	$\ \phi(\boldsymbol{\omega}^{(n)}) - \mathbf{o}\ _2^2 < R^2$	Interiors
$0 < \kappa_n < \lambda$	$\ \phi(\boldsymbol{\omega}^{(n)}) - \mathbf{o}\ _2^2 = R^2$	Boundary samples
$\kappa_n = \lambda$	$\ \phi(\boldsymbol{\omega}^{(n)}) - \mathbf{o}\ _2^2 > R^2$	Outliers

$$\text{s.t.} \quad \|\phi(\boldsymbol{\omega}^{(n)}) - \mathbf{o}\|_2^2 \leq R^2 + y_n, \quad \forall n \in \mathcal{N}, \quad (29)$$

$$y_n \geq 0, \quad \forall n \in \mathcal{N}, \quad (30)$$

where R is the radius of the sphere; $\lambda > 0$ is a controllable parameter; $\phi(\cdot)$ is the mapping function; \mathbf{o} is the center of the sphere. Since OC-SVC is used for anomaly detection, some samples lie outside the minimum sphere, i.e., the region covered by $\|\phi(\boldsymbol{\omega}^{(n)}) - \mathbf{o}\|_2^2 \leq R^2$. Thus, we introduce a nonnegative auxiliary variable y_n in constraint (29) to allow outliers, i.e., $\|\phi(\boldsymbol{\omega}^{(n)}) - \mathbf{o}\|_2^2 > R^2$ with $y_n > 0$. Nevertheless, we hope that most samples are covered by the minima sphere, so a penalty term $\lambda \sum_{n \in \mathcal{N}} y_n$ is included in the objective to reduce outlier number. Since P-SVC is convex, its optimal solution must satisfy the Karush–Kuhn–Tucker (KKT) conditions. By introducing dual variables $\boldsymbol{\kappa} \in \mathbb{R}^{|\mathcal{N}|}$ and $\mathbf{v} \in \mathbb{R}^{|\mathcal{N}|}$ for Eqs. (29) and (30), the complementary slackness is express as:

$$\kappa_n \left(R^2 + y_n - \|\phi(\boldsymbol{\omega}^{(n)}) - \mathbf{o}\|_2^2 \right) = 0, \quad \forall n \in \mathcal{N}, \quad (31)$$

$$v_n y_n = 0, \quad \forall n \in \mathcal{N}. \quad (32)$$

The stationarity condition is expressed as:

$$\mathbf{1}^\top \boldsymbol{\kappa} = 1, \quad \mathbf{o} = \sum_{n \in \mathcal{N}} \kappa_n \phi(\boldsymbol{\omega}^{(n)}), \quad \boldsymbol{\kappa} + \mathbf{v} = \lambda \cdot \mathbf{1}. \quad (33)$$

Based on the KKT conditions, we can distinguish the historical samples into three categories: interiors, boundary samples, and outliers. For example, if $\kappa_n = 0$, we have $R^2 - \|\phi(\boldsymbol{\omega}^{(n)}) - \mathbf{o}\|_2^2 = y_n$ according to Eq. (31). Based on the last constraint in Eq. (33), we also have $v_n = \lambda > 0$. In this case, Eq. (32) determines $y_n > 0$, which indicates that the sample with $\kappa_n = 0$ is an interior. Similarly, the boundary samples and outliers can be also recognized based on the value of κ_n . The criterion for distinguishing samples are summarized in Table. I. The interiors and boundary samples are regarded as safe samples, while the outliers are unsafe ones.

By substituting the stationarity condition, i.e., (33), we can also obtain the dual problem of P-SVC, as follows:

$$\begin{aligned} \max_{\boldsymbol{\kappa}} \quad & \sum_{n \in \mathcal{N}} \kappa_n K(\boldsymbol{\omega}^{(n)}, \boldsymbol{\omega}^{(n)}) - \sum_{n \in \mathcal{N}} \sum_{m \in \mathcal{N}} \kappa_n \kappa_m K(\boldsymbol{\omega}^{(n)}, \boldsymbol{\omega}^{(m)}), \\ \text{s.t.} \quad & 0 \leq \kappa_n \leq \lambda, \quad \forall n \in \mathcal{N}, \end{aligned} \quad (\text{D-SVC}) \quad (34)$$

$$\sum_{n \in \mathcal{N}} \kappa_n = 1, \quad (35)$$

where $K(\boldsymbol{\omega}^{(n)}, \boldsymbol{\omega}^{(m)}) = \phi(\boldsymbol{\omega}^{(n)})^\top \phi(\boldsymbol{\omega}^{(m)})$ is the predetermined kernel function. In this paper, we introduce a piecewise linear function proposed in [27] as our kernel function:

$$K(\boldsymbol{\omega}^{(n)}, \boldsymbol{\omega}^{(m)}) = \sum_{d \in \mathcal{D}} l_d - \|\boldsymbol{\Sigma}^{-1/2}(\boldsymbol{\omega}^{(n)} - \boldsymbol{\omega}^{(m)})\|_1, \quad (36)$$

where $\mathcal{D} = \{1, 2, \dots, D\}$ is the dimension index set of $\boldsymbol{\omega}$. Parameter $l_d = \omega_{d,\max} - \omega_{d,\min}$, where $\omega_{d,\max}$ and $\omega_{d,\min}$ are the upper and lower bound of $\boldsymbol{\omega}$ in the d -th dimension, respectively. Parameter $\boldsymbol{\Sigma}$ is the covariance matrix of the historical samples.

By solving **D-SVC**, we can get the solutions of κ_n . Then, the unsafe samples (outliers) can be recognized based on Table I, and set \mathcal{N}^{vio} can be constructed by:

$$\mathcal{N}^{\text{vio}} = \{n \mid \kappa_n = \lambda, n \in \mathcal{N}\}. \quad (37)$$

Proposition 1. *The fraction of the outliers is no more than $1/(\lambda|\mathcal{N}|)$ in OC-SVC.*

Proof: According to Table I, any outlier (unsafe sample) must have $\kappa_n = \lambda$. If the fraction of outliers exceeds $1/(\lambda|\mathcal{N}|)$, then we must have $\mathbf{1}^\top \boldsymbol{\kappa} > 1$ (note dual variable κ_n is nonnegative for all samples), which conflicts with the stationarity condition (33). This completes the proof.

Remark 3. *Proposition 1 shows that if we choose a proper value for the controllable parameter λ such that $1/(\lambda|\mathcal{N}|) \leq \epsilon^{\text{SAA}}$, then the feasibility requirement, i.e., Eq. (28) can be guaranteed. Moreover, based on this proposition, the outlier number decreases with the increase of λ . That is to say, a larger λ results in a bigger target sphere in OC-SVC, leading to a more conservative solution. Thus, here we set λ as the minimum feasible value, i.e., $1/(\epsilon^{\text{SAA}}|\mathcal{N}|)$, to ensure desirable feasibility and optimality simultaneously.*

C. Time-efficient counterpart of the robust approximation

Once the unsafe sample set \mathcal{N}^{vio} is decided, we can use sample-wise constraints (26) to replace the intractable MIP constraints (24)-(25). However, the constraint number in Eq. (26) is equal to $(|\mathcal{N}| - |\mathcal{N}^{\text{vio}}|) \cdot |\mathcal{M}| \geq |\mathcal{N}| \cdot |\mathcal{M}| \cdot (1 - \epsilon^{\text{SAA}})$. If the total sample number $|\mathcal{N}|$ is large, then the model will be computationally intractable. To address this, we further develop a time-efficient robust counterpart for Eq. (26). Specifically, we first design an uncertainty set \mathcal{U} to cover all safe samples (i.e. $\mathcal{U}^{\text{safe}} \subseteq \mathcal{U}$), then Eq. (26) can be safely approximated by the following robust constraint:

$$\max_{\boldsymbol{\omega} \in \mathcal{U}} \mathbf{a}_m(\boldsymbol{x})^\top \boldsymbol{\omega} \leq b_m(\boldsymbol{x}), \quad \forall m \in \mathcal{M}. \quad (38)$$

Here a minimum volume box is constructed as our uncertainty set. Specifically, a generic box can be expressed as:

$$\mathcal{U} = \{\boldsymbol{\omega} \mid \|\mathbf{L}\boldsymbol{\omega} - \boldsymbol{\theta}\|_\infty \leq 1\}, \quad (39)$$

where matrix \mathbf{L} and vector $\boldsymbol{\theta}$ are parameters of the box. Observing that Eq. (39) also represents a linear transformation to an unit box, the volume of the generic box defined in (39)

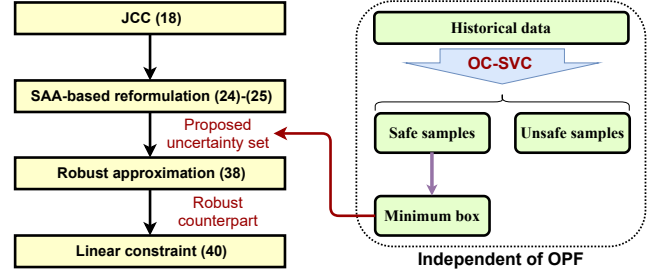


Fig. 2. The whole procedure of the proposed method. The steps in the dash-line box are independent of OPF solving, so they can be completed offline.

can be expressed as the determinant of \mathbf{L}^{-1} . Then, by solving the following optimization problem:

$$\begin{aligned} \min_{\mathbf{L}, \boldsymbol{\theta}} & -\log \det \mathbf{L}, \\ \text{s.t.} & \|\mathbf{L}\boldsymbol{\omega}^{(n)} - \boldsymbol{\theta}\|_\infty \leq 1, \quad \forall n \in \mathcal{N}/\mathcal{N}^{\text{vio}}, \end{aligned} \quad (\mathbf{P-U})$$

we can get the target minimum volume box that can cover all the safe samples. Once the minimum volume box is found, Eq. (38) can be replaced by its counterpart:

$$\|\mathbf{L}^{-1} \mathbf{a}_m(\boldsymbol{x})\|_1 \leq b_m(\boldsymbol{x}) - \mathbf{a}_m(\boldsymbol{x})^\top \mathbf{L}^{-1} \boldsymbol{\theta}, \quad \forall m \in \mathcal{M}. \quad (40)$$

Since Eq. (40) only introduces $|\mathcal{M}|$ constraints no matter how many safe samples we have, it is much more computationally efficient compared to Eq. (26).

D. Summary of the proposed method

Considering that the power flow model, i.e., Eqs. (6)-(7) is linear, the objective (1) can be expressed as:

$$\mathbb{E} \left(\sum_{t \in \mathcal{T}} EC_t \right) = \sum_{t \in \mathcal{T}} EC_t(\boldsymbol{x}_t, \boldsymbol{\omega}_t^{\text{avg}}), \quad (41)$$

where $\boldsymbol{\omega}_t^{\text{avg}} = \mathbb{E}(\boldsymbol{\omega}_t)$. By using the proposed robust approximation (40) to replace JCC (18), **P2** is reformulated as:

$$\begin{aligned} \min_{\boldsymbol{x}_t, \forall t \in \mathcal{T}} & \text{Eq. (41)}, \\ \text{s.t.} & \text{Eqs. (2)-(3), (5)-(7), (10)-(14), (17), and (40)}. \end{aligned} \quad (\mathbf{P3})$$

The whole procedure of the proposed method is summarized in Fig. 2. First, we apply the SAA to reformulate JCC (16) into a mixed-integer programming with deterministic sample-wise constraints. Second, the OC-SVC is introduced to identify safe and unsafe samples so that the binary variables in SAA can be predetermined. Considering that size of sample-wise constraints is too large, we further design a minimum volume box as our uncertainty set to cover all safe samples. Then, by requiring all OPF constraints to be robust for the uncertainty set, the previous large-scale sample-wise constraints can be replaced by a small number of robust constraints. As a result, the proposed joint chance constrained OPF problem **P2** is approximated by a simple robust linear programming **P3**.

IV. CASE STUDY

A. Simulation set up

We implement a case study based on the IEEE 13-bus system with two WTs (WT1 and WT2) and two ESSs (ESS1 and ESS2), as shown in Fig. 3. The resistance r_{ij} , reactance

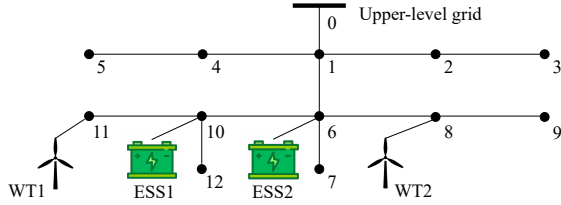


Fig. 3. Structure of the test system.

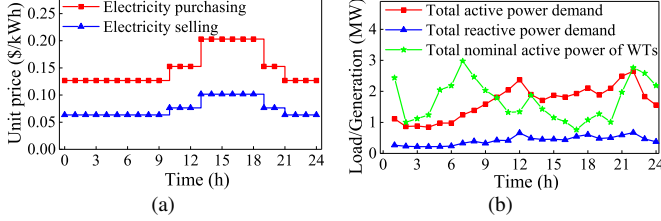


Fig. 4. (a) Electricity prices and (b) total active/reactive power demand and nominal active power output of WTs.

x_{ij} , and maximum allowable power flow S_{ij}^{\max} of each branch have been uploaded in [28]. The optimization horizon and time step Δt are 24h and 1h, respectively. Fig. 4 shows the unit prices for electricity purchasing/selling, total active/reactive power demands, and total nominal active power output of all WTs. Other parameters summarized in Table II.

Various distributions have been used in different published works (i.e. Gaussian distribution in [4], Beta distribution in [29], and Weibull distribution in [30]) to describe the uncertainty from wind generation. To demonstrate the ability of the proposed method for handling arbitrarily distributed uncertainties, we implement three cases with different sample generators to simulate historical data, i.e., Case 1 with Gaussian distribution, Case 2 with Beta distribution and Case 3 with Weibull distribution. In each case, 500 samples are generated as the training set to construct the uncertainty set for the proposed joint chance-constrained OPF model. Another 10,000 samples are generated as the testing set to validate the solutions' feasibility performance. The detailed parameter setting and all generated samples can be found in [28].

All numerical experiments are tested on an Intel(R) 8700 3.20GHz CPU with 16 GB memory. GUROBI combined with CVXPY are employed to solve the optimization problem.

B. Benchmarks

We implement four models to verify the superiority of the proposed approach, as follows:

- 1) **M1**: The proposed approach, i.e. **P3**;
- 2) **M2**: The Bonferroni approximation used in [10]–[12];
- 3) **M3**: The scenario approach used in [16], [18], [19];

TABLE II
PARAMETERS IN CASE STUDY

Parameters	Value
Maximum value of the square of bus voltage U^{\max}	$(1.05\text{p.u.})^2$
Minimum value of the square of bus voltage U^{\min}	$(0.95\text{p.u.})^2$
Ratio of WTs' active power outputs to reactive ones ψ_t	0.1
Maximum energy storage capacity of ESSs E^{\max}	0.5MW
Minimum energy storage capacity of ESSs E^{\min}	0
Confidence parameter β in Lemma 1	0.01

TABLE III
DESCRIPTIONS OF THE IMPLEMENTED MODELS

Models	Reformulations	Constraint Numbers	Integer
M1	Eq. (40)	$ \mathcal{M} $	No
M2	Eq. (42)	$ \mathcal{M} $	No
M3	Eq. (45)	$ \mathcal{M} $	No
M4	Eqs. (24)–(25)	$ \mathcal{N} \cdot \mathcal{M} + 1$	Yes

¹ Column **Reformulations** refers to the reformulations of the JCC.

² Column **Integer** refers whether integer variables are required by the corresponding model.

4) **M4**: The conventional SAA used in [21], [22].

The only differences among **M1**–**M4** are the ways to reformulate JCC (16), which are summarized in Table. III.

In **M2**, the original JCC is decomposed into:

$$\begin{aligned} \mathbb{P}(\mathbf{a}_m(\mathbf{x})^\top \boldsymbol{\omega} \leq b_m(\mathbf{x}), \forall m \in \mathcal{M}) &\geq 1 - \epsilon \\ \Rightarrow \mathbb{P}(\mathbf{a}_m(\mathbf{x})^\top \boldsymbol{\omega} \leq b_m(\mathbf{x})) &\geq 1 - \epsilon_m, \forall m \in \mathcal{M}. \end{aligned} \quad (42)$$

Here we adopt the manner used in references [10]–[12] to set the value of ϵ_m as $\epsilon/|\mathcal{M}|$. Then, based on Gaussian assumption, these ICCs can be reformulated into second-order cone constraints².

The scenario approach, **M3**, uses a scenario set containing N^{SA} randomly drawn samples, i.e., $\{\boldsymbol{\omega}^{(n)}\}_{n=1}^{N^{\text{SA}}}$, to approximate the original JCC (21) as:

$$h(\mathbf{x}, \boldsymbol{\omega}^{(n)}) \leq 0, \quad \forall n \in \{1, 2, \dots, N^{\text{SA}}\}. \quad (43)$$

If the scenario number N^{SA} satisfy the following constraint:

$$N^{\text{SA}} \geq \frac{1}{\epsilon} \frac{e}{e-1} \left(\ln \frac{1}{\beta} + 2D_\omega - 1 \right), \quad (44)$$

then the optimal solution of Eq. (43) will be also feasible to JCC (21) with confidence at least $1 - \beta$ [16]. Here e is the Euler number and D_ω is the dimension of uncertainty $\boldsymbol{\omega}$. The scenario numbers required by **M3** with different risk parameters are illustrated in Fig. 5(a). To improve computational efficiency, references [18], [19] further constructed minimum volume box uncertainty sets \mathcal{U}^{box} to cover all scenarios. Then, Eq. (43) is converted into a robust constraint:

$$\max_{\boldsymbol{\omega} \in \mathcal{U}^{\text{box}}} h(\mathbf{x}, \boldsymbol{\omega}) \leq 0. \quad (45)$$

The major difference between the proposed method **M1** and **M3** are as follows: **M3** requires that all constraints should be satisfied for all randomly selected samples, as shown in Fig. 5(B). In **M1**, some samples are recognized as unsafe ones and may violate some constraints.

C. Case 1: Gaussian distributed uncertainties

1) *Visualization of uncertainty sets*: Fig. 6 visualize the box uncertainty sets in the proposed method **M1** and scenario approximation **M3**. No matter how large the risk parameter ϵ is, the box in the proposed method always covers the space where the density of samples is high. In **M3**, the uncertainty set will be very large and introduce unnecessary conservativeness if some extreme samples (i.e. scenarios) are

²In fact, the uncertainty may not follow Gaussian distribution. Thus, instead of the Gaussian assumption, distributionally robust chance-constrained (DRCC) methods may be more applicable. However, DRCC is usually more conservative. The motivation of using the Gaussian assumption here is to highlight the bad optimality performance of **M3**.

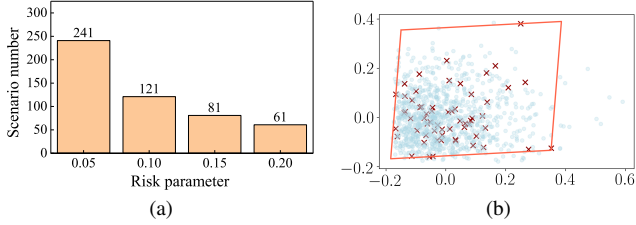


Fig. 5. (a) The scenario numbers with different risk parameters and (b) an example uncertainty set in **M3**. In (b), the red crosses represent the randomly chosen scenarios, while the light blue dots denote the samples that are not chosen. The red box (uncertainty set) is the minimum box that can cover all chosen scenarios.

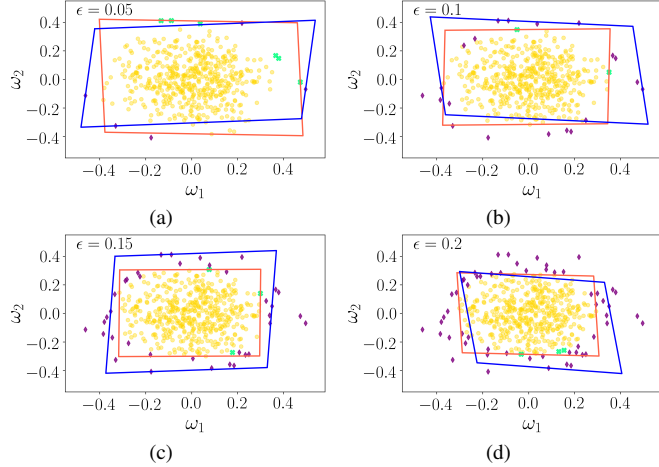


Fig. 6. Uncertainty sets obtained by the proposed approach **M1** (red box) and scenario approximation **M3** (blue box) with (a) $\epsilon = 0.05$, (b) $\epsilon = 0.10$, (c) $\epsilon = 0.15$, and (d) $\epsilon = 0.20$ in Case 1 with Gaussian distributed uncertainties. The gold dots, green crosses, and purple diamonds represent the internals, boundary samples, and outliers, which are distinguished by OC-SVC.

are covered. Unfortunately, since all scenarios are randomly drawn, it is often the case. For instance, in Fig. 6(b), the rightmost sample is chosen as the scenarios by **M3**. Thus, a very large box uncertainty set is needed to cover these two samples. Unlike **M3**, the proposed method introduces OC-SVC to decide which samples need to be covered. By solving **P-SVC**, the outliers that are far apart from the majority of samples can be recognized. Compared to **M3**, the covered samples are more concentrated, so they can be covered by a smaller box. These results indicate that the proposed method can achieve better optimality than **M3**.

2) *Optimality, time-efficiency, and feasibility*: Fig 7 illustrates the results of energy costs, solving times, maximum violation probabilities, and utilization rates of wind power obtained by different models under Gaussian distributed uncertainties. Here “M4(60s)” indicates that the corresponding results are obtained by **M4** at solving time equals to 60s, while “M4(Final)” represents the final solutions that reach global optima or solving time limit (3600s). Among all methods, the energy cost of the proposed method is relatively low and only higher than that of **M4(Final)** no matter how large the risk parameter ϵ is. According to Eq. (42), if the Bonferroni approximation **M2** is used to handle JCC, then the risk parameter of each ICC, i.e., ϵ_m , will be very small, especially when a large number of constraints are jointly considered in one JCC. Thus, **M2** derives a much more conservative

solution compared to the proposed one. As mentioned in the discussion on Fig. 6, **M3** needs a large box to cover the scenarios that are far away from the majority of samples, so the energy-efficiency of **M3** is worse than the proposed one. Although the final solution of the conventional SAA **M4**, i.e., the results of **M4(Final)**, can achieve better optimality compared to the proposed one, its solving time is several orders of magnitude larger. For example, in all cases, the solving time of the proposed method is less than 0.1s, while **M4(Final)** needs to spend hundreds or even thousands of seconds to find its optimal solution. This is because **M4** needs to introduce numerous intractable binary variables to reformulate the original JCC, while the proposed method can directly convert the JCC into a small number of tractable linear constraints. Moreover, the solution of **M4(60s)** is still more conservative than that of the proposed one. In addition, it takes at least 40s for **M4** to find a feasible solution. These results confirm the excellent optimality and time efficiency of the proposed method.

The maximum violation probabilities of all models are lower than the given risk parameter. We introduce probability guarantees for both the SAA (**M1** and **M4**) and scenario approximation (**M3**), while the Bonferroni approximation (**M2**) is an inner approximation of the original JCC. Thus, even though the solutions of all methods are derived based on the training set with only 500 samples, the feasibility can still be maintained in the testing set with 10,000 samples. These results demonstrate the desirable feasibility of the proposed method.

As aforementioned, the proposed method can achieve better optimality than **M2**, and **M3**. Therefore, the proposed one can better promote the utilization of wind power. For example, the utilization rate of the proposed method is around 2% higher than **M2** and **M3**. Although **M4(Final)** can derive higher utilization rate results, it is impractical considering its computational burden. In fact, the utilization rate of **M4(60s)** is still lower than that of the proposed one.

D. Case 2: Beta distributed uncertainties

1) *Visualization of uncertainty sets*: Fig. 8 shows the uncertainty sets established by **M1** and **M3** with Beta distributed uncertainties. Similar to Case 1, the box uncertainty set of **M3** needs to cover some extreme scenarios, e.g., the leftmost two samples in Fig. 8(b) and (c), while the samples covered by the box of **M1** are more concentrated. Thus, the uncertainty set of **M3** is significantly larger than that of **M1**.

2) *Optimality, feasibility and time-efficiency*: The results of different models in Case 2 with Beta distributed uncertainties are illustrated Fig. 9. **M4(Final)** still achieves the most energy-efficient solution. However, since its solving time is four or five orders of magnitude larger than those in **M1**, **M2**, and **M3**, it is not applicable in most practical cases. In the other methods, the proposed one achieves the best optimality performance with the highest utilization rate of wind power. The corresponding maximum probability violation is always smaller than the given risk parameter. Moreover, its solving time is only around 0.06s. These results further confirm the superiority of the proposed method on optimality and computational efficiency.

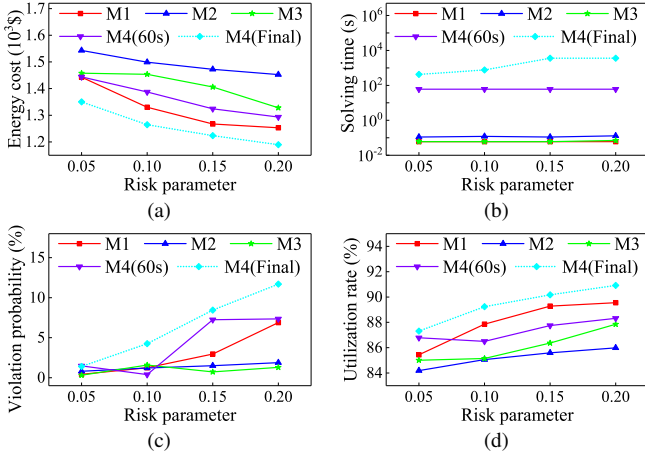


Fig. 7. Results of (a) energy costs, (b) solving times, (c) maximum violation probability, and (d) utilization rate of wind powers with different risk parameters in Case 1. Symbol “M4(60s)” indicates that the corresponding results are obtained at solving time equals to 60s. Symbol “M4(Final)” represents the final solutions of **M4** (i.e. the solutions achieving global optima or reaching solving time limit). In Case 1, it takes at least 40s for **M4** to find the first feasible solution no matter how large the risk parameter is.

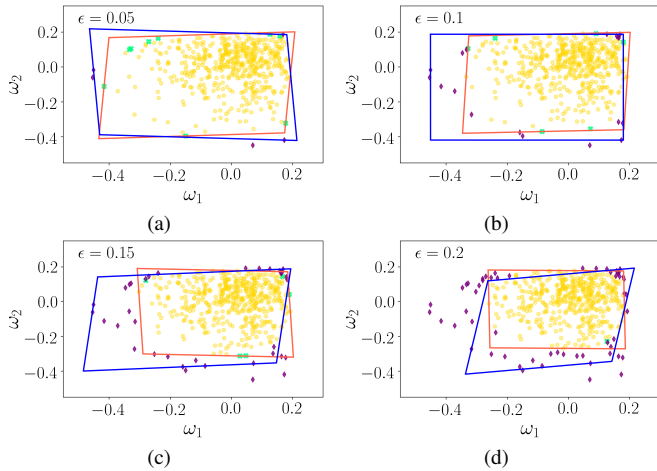


Fig. 8. Uncertainty sets obtained by the proposed approach **M1** (red box) and scenario approximation **M3** (blue box) with (a) $\epsilon = 0.05$, (b) $\epsilon = 0.10$, (c) $\epsilon = 0.15$, and (d) $\epsilon = 0.20$ in Case 2 with Beta distributed uncertainties.

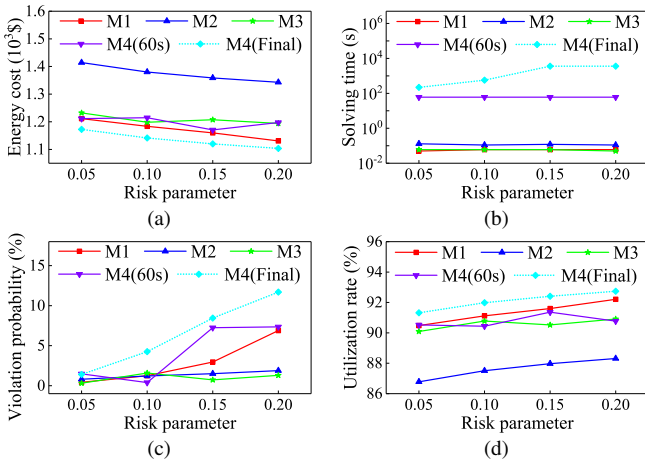


Fig. 9. Results of (a) energy costs, (b) solving times, (c) maximum violation probability, and (d) utilization rate of wind powers with different risk parameters in Case 2. In Case 2, it takes at least 35s for **M4** to find the first feasible solution no matter how large the risk parameter is.

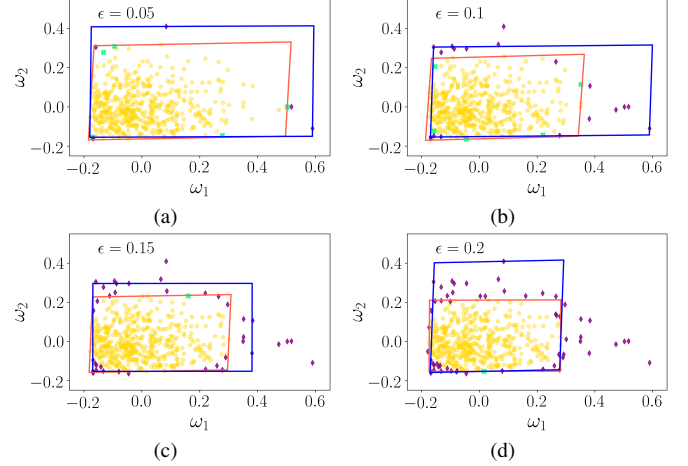


Fig. 10. Uncertainty sets obtained by the proposed approach **M1** (red box) and scenario approximation **M3** (blue box) with (a) $\epsilon = 0.05$, (b) $\epsilon = 0.10$, (c) $\epsilon = 0.15$, and (d) $\epsilon = 0.20$ in Case 3 with Weibull distributed uncertainties.

E. Case 3: Weibull distributed uncertainties

1) *Visualization of uncertainty sets:* Fig. 10 demonstrates the uncertainty sets constructed by **M1** and **M3** in Case 3 with Weibull distributed uncertainties. In all cases, the box uncertainty set of **M3** is obviously larger than that of **M1**. As aforementioned, since the scenarios in **M3** are randomly selected, some marginal samples may be chosen into the scenario set, e.g., the uppermost and rightmost samples in 10(a). A large box is required so that all scenarios can be covered. Unlike **M3**, the proposed method **M1** leverages OC-SVC to identify the marginal samples and treat them as outliers, resulting in a smaller box uncertainty set.

2) *Optimality, feasibility and time-efficiency:* The energy costs, solving times, maximum violation probabilities, and utilization rates of wind power in Case 3 are summarized in Fig. 11. Similar to the results in Cases 1 and 2, the proposed method **M1** derives a more energy-efficient solution compared to the Bonferroni approximation **M2** and scenario approximation **M3**. Accordingly, the utilization rate of wind power in **M1** is also higher than those in **M2** and **M3**. Moreover, the solving time of **M1** is only around 0.06s in all cases, while it takes 60s for the conventional SAA **M4** to obtain a comparable solution. The maximum violation probabilities of all methods are lower than the risk parameter, which indicates that all methods can guarantee proper feasibility.

In summary, the proposed method can always achieve better optimality than the widely used Bonferroni approximation **M2** and scenario approach **M3** in all three cases. Although **M4** can achieve comparable optimality performance, the computational efficiency is much worse compared to **M1**. These results validate the benefits of the proposed method.

V. CONCLUSIONS

In this work, a time-efficient joint chance-constrained OPF model is proposed to ensure the operational security of distribution system with uncertainties. To deal with the intractable JCC, a learning-based robust approximation method is proposed. The proposed method first adopts SAA to convert the

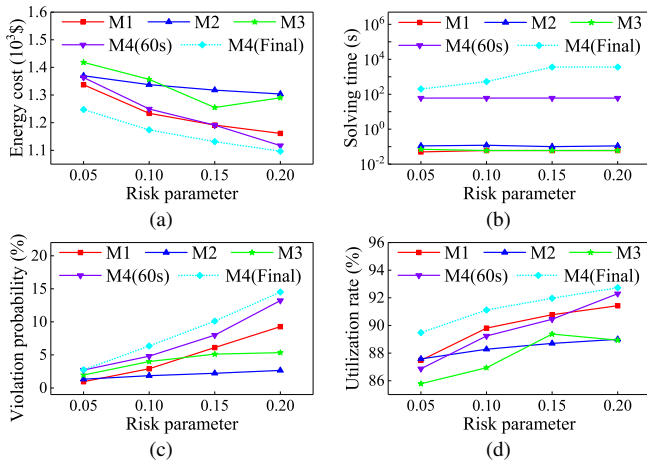


Fig. 11. Results of (a) energy costs, (b) solving times, (c) maximum violation probability, and (d) utilization rate of wind powers with different risk parameters in Case 3. In Case 3, it takes at least 39s for M4 to find the first feasible solution no matter how large the risk parameter is.

JCC into deterministic sample-wise constraints with many binary variables. Then, the OC-SVC is introduced to identify safe and unsafe samples so that the computationally intractable binary variables can be predetermined. To further improve the computational performance, a robust approximation is designed to convert the huge number of sample-wise constraints into only a few robust constraints. As a result, the original complex joint chance-constrained OPF model is formulated into a simple linear form. Moreover, since the proposed model is data-driven, it is applicable to arbitrarily distributed uncertainties. Numerical experiments based on an IEEE 13 bus system indicate that the proposed method derives a more energy-efficient solution than the widely used Bonferroni approximation and scenario approach. Moreover, the solving time of the proposed model is always lower than 0.1s, which also confirms the great computational efficiency of the proposed method. Case studies based on various distributed uncertainties also confirm the ability of the proposed method for handling arbitrarily distributed uncertainties.

REFERENCES

- [1] Y. Tang, K. Dvijotham, and S. Low, "Real-time optimal power flow," *IEEE Transactions on Smart Grid*, vol. 8, no. 6, pp. 2963–2973, 2017.
- [2] Y. Xu, M. Korkali, L. Mili, J. Valinejad, T. Chen, and X. Chen, "An iterative response-surface-based approach for chance-constrained ac optimal power flow considering dependent uncertainty," *IEEE Transactions on Smart Grid*, vol. 12, no. 3, pp. 2696–2707, 2021.
- [3] X. Geng and L. Xie, "Data-driven decision making in power systems with probabilistic guarantees: Theory and applications of chance-constrained optimization," *Annual reviews in control*, vol. 47, pp. 341–363, 2019.
- [4] D. Bienstock, M. Chertkov, and S. Harnett, "Chance-constrained optimal power flow: Risk-aware network control under uncertainty," *Siam Review*, vol. 56, no. 3, pp. 461–495, 2014.
- [5] E. Dall'Anese, K. Baker, and T. Summers, "Chance-constrained ac optimal power flow for distribution systems with renewables," *IEEE Transactions on Power Systems*, vol. 32, no. 5, pp. 3427–3438, 2017.
- [6] Y. Yang, W. Wu, B. Wang, and M. Li, "Analytical reformulation for stochastic unit commitment considering wind power uncertainty with gaussian mixture model," *IEEE Trans. Power Syst.*, vol. 35, no. 4, pp. 2769–2782, 2020.
- [7] F. Qi, M. Shahidehpour, Z. Li, F. Wen, and C. Shao, "A chance-constrained decentralized operation of multi-area integrated electricity–natural gas systems with variable wind and solar energy," *IEEE Trans. Sustain. Energy*, vol. 11, no. 4, pp. 2230–2240, 2020.
- [8] W. Xie and S. Ahmed, "Distributionally robust chance constrained optimal power flow with renewables: A conic reformulation," *IEEE Trans. Power Syst.*, vol. 33, no. 2, pp. 1860–1867, 2018.
- [9] W. Chen, M. Sim, J. Sun, and C.-P. Teo, "From cvar to uncertainty set: Implications in joint chance-constrained optimization," *Operations research*, vol. 58, no. 2, pp. 470–485, 2010.
- [10] Y. Cao, Y. Tan, C. Li, and C. Rehtanz, "Chance-constrained optimization-based unbalanced optimal power flow for radial distribution networks," *IEEE Trans. Power Deliv.*, vol. 28, no. 3, pp. 1855–1864, 2013.
- [11] A. Hassan, R. Mieth, M. Chertkov, D. Deka, and Y. Dvorkin, "Optimal load ensemble control in chance-constrained optimal power flow," *IEEE Trans. Smart Grid*, vol. 10, no. 5, pp. 5186–5195, 2018.
- [12] B. Odetayo, M. Kazemi, J. McCormack, W. D. Rosehart, H. Zareipour, and A. R. Seifi, "A chance constrained programming approach to the integrated planning of electric power generation, natural gas network and storage," *IEEE Trans. Power Syst.*, vol. 33, no. 6, pp. 6883–6893, 2018.
- [13] K. Baker and B. Toomey, "Efficient relaxations for joint chance constrained ac optimal power flow," *Electr. Power Syst. Res.*, vol. 148, pp. 230–236, 2017.
- [14] K. Baker and A. Bernstein, "Joint chance constraints in ac optimal power flow: Improving bounds through learning," *IEEE Trans. Smart Grid*, vol. 10, no. 6, pp. 6376–6385, 2019.
- [15] D. Bertsimas, V. Gupta, and N. Kallus, "Data-driven robust optimization," *Math Program*, vol. 167, no. 2, pp. 235–292, 2018.
- [16] L. Roald and G. Andersson, "Chance-constrained ac optimal power flow: Reformulations and efficient algorithms," *IEEE Transactions on Power Systems*, vol. 33, no. 3, pp. 2906–2918, 2018.
- [17] X. Geng, L. Xie, and M. Sadegh Modarresi, "A general scenario theory for security-constrained unit commitment with probabilistic guarantees," *arXiv e-prints*, pp. arXiv–1910, 2019.
- [18] A. Venzke, L. Halilbasic, U. Markovic, G. Hug, and S. Chatzivasileiadis, "Convex relaxations of chance constrained ac optimal power flow," *IEEE Transactions on Power Systems*, vol. 33, no. 3, pp. 2829–2841, 2018.
- [19] A. Venzke and S. Chatzivasileiadis, "Convex relaxations of probabilistic ac optimal power flow for interconnected ac and hvdc grids," *IEEE Transactions on Power Systems*, vol. 34, no. 4, pp. 2706–2718, 2019.
- [20] Q. Wang, Y. Guan, and J. Wang, "A chance-constrained two-stage stochastic program for unit commitment with uncertain wind power output," *IEEE Trans. Power Syst.*, vol. 27, no. 1, pp. 206–215, 2012.
- [21] X. Cao, J. Wang, and B. Zeng, "Networked microgrids planning through chance constrained stochastic conic programming," *IEEE Transactions on Smart Grid*, vol. 10, no. 6, pp. 6619–6628, 2019.
- [22] Y. Zhang, J. Wang, B. Zeng, and Z. Hu, "Chance-constrained two-stage unit commitment under uncertain load and wind power output using bilinear benders decomposition," *IEEE Transactions on Power Systems*, vol. 32, no. 5, pp. 3637–3647, 2017.
- [23] Z. Wang, B. Chen, J. Wang, M. M. Begovic, and C. Chen, "Coordinated energy management of networked microgrids in distribution systems," *IEEE Trans. Smart Grid*, vol. 6, no. 1, pp. 45–53, 2014.
- [24] S. H. Low, "Convex relaxation of optimal power flow—part i: Formulations and equivalence," *IEEE Transactions on Control of Network Systems*, vol. 1, no. 1, pp. 15–27, 2014.
- [25] M. C. Campi and S. Garatti, "A sampling-and-discarding approach to chance-constrained optimization: feasibility and optimality," *Journal of optimization theory and applications*, vol. 148, no. 2, pp. 257–280, 2011.
- [26] M. Bicego and M. A. Figueiredo, "Soft clustering using weighted one-class support vector machines," *Pattern Recognition*, vol. 42, no. 1, pp. 27–32, 2009.
- [27] C. Shang, X. Huang, and F. You, "Data-driven robust optimization based on kernel learning," *Comput Chem Eng*, vol. 106, pp. 464–479, 2017.
- [28] "Samples." [Online]. <https://github.com/elouchsola/SVCBasedOPF>.
- [29] H. Bludszweit, J. A. Dominguez-Navarro, and A. Llombart, "Statistical analysis of wind power forecast error," *IEEE Trans. Power Syst.*, vol. 23, no. 3, pp. 983–991, 2008.
- [30] P. Zhang and S. Lee, "Probabilistic load flow computation using the method of combined cumulants and gram-charlier expansion," *IEEE Trans. Power Syst.*, vol. 19, no. 1, pp. 676–682, 2004.